Attitude Determination and Control System for University of Illinois Nanosatellite Architecture

Design Document

ECE 445 - Group 1

Rick Eason - reason2@illinois.edu
Srikar Nalamalapu - svn3@illinois.edu
Shamith Achanta - shamith2@illinois.edu

University of Illinois Urbana-Champaign - Electrical and Computer Engineering Department

February 24, 2022

Contents

1 Introduction

1.1 Problem

The University of Illinois Aerospace Engineering department's Laboratory for Advanced Space Systems at Illinois (LASSI) develops nanosatellites for the University of Illinois. Their next-generation satellite architecture is currently in development, however the core bus does not contain an Attitude Determination and Control (ADCS) system.

An ADCS system is a spacecraft subsystem that is capable of performing controlled changes and determination of a spacecraft's attitude.

1.2 Solution

Design an IlliniSat-0 specification compliant ADCS module. This module shall be capable of sensing the Earth's magnetic field, sensing the body rotation rate of the module, executing algorithms to generate control solutions, and actuate those solutions using magnetorquer coils.

A magnetorquer coil is a solenoid coil that can be commanded to generate a field of a certain strength and direction. This field interacts with Earth's magnetic field and generates a body torque on the spacecraft [1]. This form of solid-state attitude control is very weak, and as such is only used on small spacecraft.

In order for an ADCS system to be useful to LASSI, the system must be compliant with their modular spacecraft bus architecture. This module shall be physically, electrically, and digitally compliant with LASSI specifications. One of the important factors in the design of magnetorquer devices is the shape and size of the driving coils. The coils must be simultaneously efficient at producing a magnetic field, and be small enough to fit inside, and not waste space in, a nanosatellite bus. To that end, we have analyzed contemporary solutions, as well as studies of the optimization of magnetorquers [2], to develop driving coil geometries that are both compact and make efficient use of the current being fed through them.

1.3 Visual Aid

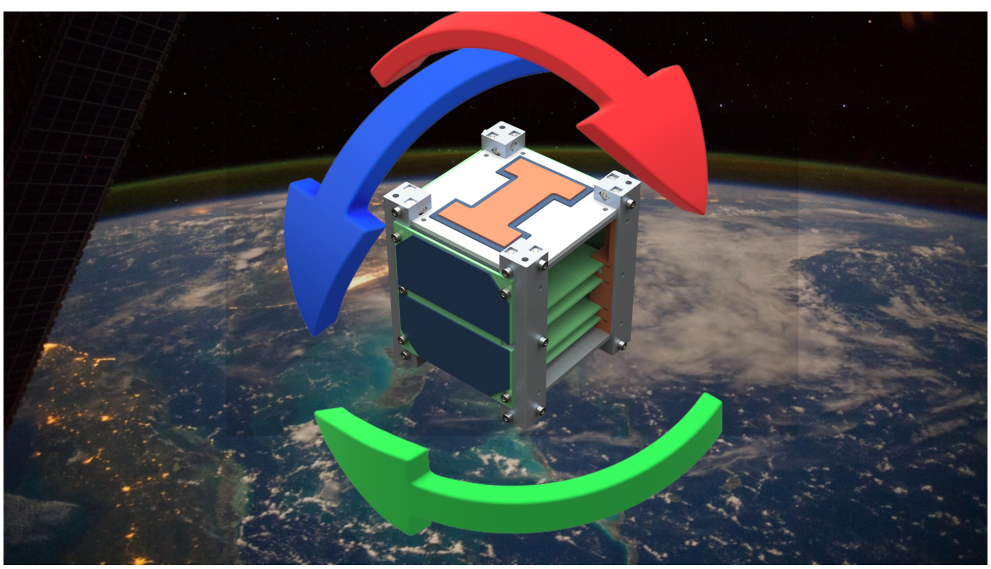

Figure 1: A render of the IlliniSat-0 spacecraft above Earth, with arrows indicating the three body rotational axes. On the right, downward facing side an open face into the spacecraft shows the PCB stackup, our device will be inside the spacecraft on this stack.

1.4 High-Level Requirements

Table 1: Requirements and verification table for system high-level requirements.

Requirement	Verification
1. The system shall be compliant with LASSI IlliniSat-0 specifications for spaceflight hardware.	**1A.** Design board with LASSI provided mechanical drawings and related pattern files. **1B.** Select external interface parts, such as serial transceivers and stack connectors, from LASSI specified part numbers. **1C.** Completed hardware shall draw no more than 2 amps of current from the 3.3 volt power supply rail at maximum load. **1D.** Completed hardware shall be capable of accepting commands from the CAN and RS-422 serial interfaces. **1E.** Completed hardware shall be capable of sending telemetry and attitude data over the CAN and RS-422 serial interfaces.
2. The system shall enter a fault state when abnormal performance is detected.	**2A.** Ensure the system transitions to a fault state when a strong permanent magnet is brought within 3 centimeters of the magnetometer. **2B.** Ensure the system transitions to a fault state when the board is rotated at greater than 100 degrees per second. **2C.** Ensure the system transitions to a fault state when the constant-current drivers are shorted by a 5cm copper wire bridging the coil solder connections. **2D.** Ensure the system transitions to a fault state when the actuator coils are disconnected, leaving an open circuit through the constant-current drive.
3. The system shall accurately read the local magnetic field vector and rotation rate.	**3A.** Using the STM32 under the control of a hardware debugger, read the magnetic field strength values from the magnetometer. Ensure they remain within 5% of values returned by external magnetometers. **3B.** Using the STM32 under the control of a hardware debugger, read the rotation rates from the gyroscope. Ensure they remain within 5% pf values returned by external gyroscopes.
4. The system shall be capable of generating a certain magnetic field in each of the system's three principle orthogonal vectors.	**4A.** Using the STM32 under the control of a hardware debugger, command a coil to generate a field. Measure the field with an external magnetometer placed centered on the opening of the coil structure, within 5mm of the coil.Verify that the field strength commanded is within 5% of the field strength commanded. Repeat on all 3 coils.

2 Design

2.1 Block Diagram

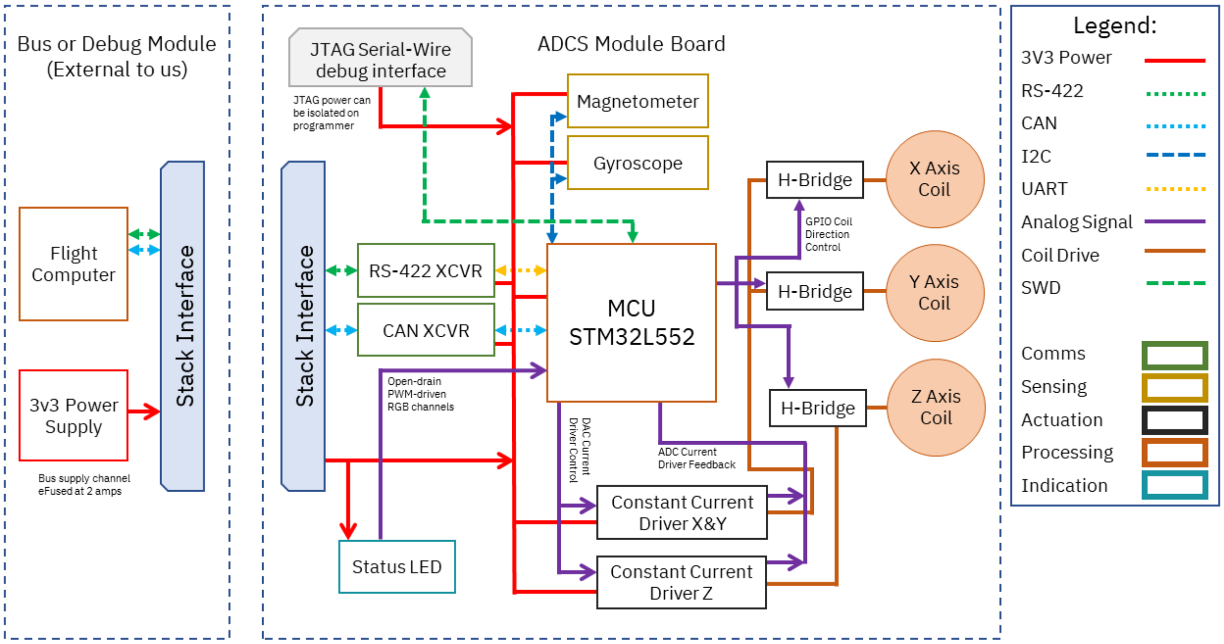

Figure 2: Updated block diagram. All connections are of the legend-specified type unless otherwise noted.

Figure 2 is a visual diagram indicating the different subsystems on the device, as well as their interfacing. All power is DC 3.3V, this power is regulated and e-fused external to our system. RS-422 and CAN are both external interface serial transceivers and operate at up to 1 MBaud. I^2C and UART are both contained internal to our system. UART operates at up to 1 MBaud, and I^2C operates at the standard I^2C high speed rate of 400 kbps. All analog signals are low-speed DC level signals. Serial Wire Debug (SWD) is a standard modified form of JTAG which is used to program and debug the MCU.

The status LED module is an RGB LED module is low-side driven by three open-drain channels on the MCU, one for each color. Each of the three channels is driven by an independent PWM timer peripheral which allows firmware control over the effective color of the indicator. This allows for faster communication of state and faults to us during testing.

2.2 Constant-Current Drivers

The constant-current drivers are a critical part of this system. Without the ability to reliably and controllably draw current through the magnetorquer coils, a control solution cannot be implemented and the module will not meet its desired functionality. We performed an analysis on several different constant-current architectures and determined that an op-amp current-feedback architecture was the best option for our purposes [3].

There are two independently controlled constant-current drivers on the module, one which drives current through the X and Y axis coils, and one that drives current through the Z axis coil. This fragmentation is due to the fact that the X and Y axis coils are identical, but the Z axis coil is shaped differently and therefore has a different set of characteristics. Because the constant-current drivers are tuned for a certain amount of Ohmic resistance in the coils, the Z axis driver must be tuned differently in order to present a high dynamic-range control regime to the microcontroller. Analysis of this is done in detail in section 2.7.

The drivers are given a set point by the DACs built into the MCU. The driver then automatically seeks that set current and holds there until a new set point is given by the MCU. The current feedback signal is tapped by an ADC channel on the MCU for firmware feedback capability. The ADC presents an external impedance of 50,000 Ohms and does not sink current from the measured system.

Requirements and Verification

Table 2: Requirements and Verification Table for Constant-Current Driver Subsystem

Requirement	Verification
1. The drivers shall drive no more than 250 milliamps of current through the coils.	**1A.** Measure the resistance of the coil while it is isolated from the board. Using a multimeter, measure the voltage across the coil when the driver is set to maximum current. Use Ohm's law to calculate the current and ensure it is bellow 250 mA.
2. The MCU shall be able to read the current driven through the coils for a given set point.	**2A.** Measure the resistance of the coil while it is isolated from the board. Using a multimeter, measure the voltage across the coil when the driver is set to a known set point. Use Ohm's law to calculate the current and ensure it is within 5% of the targeted set point.
3. The MCU shall be able to perform a full-range sweep of each current driver and calibrate itself to the given coil's current response.	**3A.** Using the STM32 debugger, command the MCU to perform a calibration sweep of the driver. Measure the resistance of the coil while it is isolated from the board. Calculate the correct current of the coil at 4 arbitrary, but roughly evenly spaced out, set points. Compare the measured current of the coil to the targeted value before and after the test. Ensure the accuracy of the test currents improves. In the case of the 'before' test being already calibrated, ensure the accuracy of the results does not deteriorate.

2.3 Stack Interface and Serial Transceivers

In order for subsystems of the satellite to communicate with each other and share resources, a standard board stacking connector and pinout was determined and set by LASSI specifications. Due to formatting constraints, the specification diagram for the stack connector is not included in this document.

In order to accommodate differences in subsystem data volume and rate requirements, the LASSI specification calls for two different serial interfaces on each module. These are RS-422, a differential signalled form of UART, and CAN bus, a multi-drop packet protocol commonly used in industrial and automotive applications. Both RS-422 and CAN interfaces require dedicated transceiver ICs in order to operate correctly. The RS-422 transceiver will communicate to the MCU over a dedicated UART line and the CAN transceiver will communicate over the MCU dedicated CAN interface. The MCU has a CAN interface but requires the external transceiver to drive the lines correctly.

The higher-layer protocol that will be used over both of these interfaces is the same. It is a LASSI specification modification of the AX-25 protocol and MessagePack. This protocol is complete and being implemented in other systems. We will develop firmware to support the use of this protocol.

Requirements and Verification

Table 3: Requirements and Verification Table for External Interface Subsystem

Requirement	Verification
1. The stack interface shall physically and electrically conform to LASSI specifications.	**1A.** Use of standardized connectors, the Samtec ERM/F-8 series, and standardized footprint positioning will ensure the mechanical matching. **1B.** Compliance with pin matching and passthrough of unrelated pins will be enforced during board design.
2. The RS-422 interface shall be capable of bi-directional serial communication to the MCU at less than or equal to 1 MBaud.	**2A.** Connect an external RS-422 interface to the device, enter a serial test mode, and ensure that accurate data transfer occurs at the tested datarates.
3. The CAN bus interface shall be capable of bi-directional serial communication to the MCU at less than or equal to 1 MBaud.	**3A.** Connect an external CAN interface to the device, enter a serial test mode, and ensure that accurate data transfer occurs at the tested datarates.

2.4 IMUs

In order to perform control operations, sensor input must be acquired. For the purposes of this device, those sensors consist of a three-axis gyroscope, and a three-axis magnetometer. Several important factors must be considered when selecting specific parts for this system; the devices must be extremely sensitive in order to detect the very weak magnetic field around the planet, and very low rotation rates, and that those fields and rates are very low-frequency signals.

Due to increased demand for small and high-accuracy inertial measurement capabilities, driven primarily by the wearable consumer technology market, modern IMUs are dramatically more capable than their contemporaries of even 5 years ago. Both of the selected devices contain configurable internal low-pass filters, which will reduce signal processing load on the microcontroller. Both devices also have configurable sampling rates and gain, allowing for improved accuracy.

Due to the ongoing component shortages, it was not possible to obtain a single-device all-in-one IMU with sufficient sensitivity for our application. As such, a discrete magnetometer and gyroscope have been selected. An analysis of the sensitivity of the magnetometer is performed in section 2.7.1. Both devices communicate over I^2C and will be sharing a bus to the MCU. Initialization and setup of the devices is done through I^2C by writing to control registers and verifying certain values in read-only registers. The magnetometer once powered on includes a continuous mode at different operating frequencies. This will be a useful feature for retrieving continuous data from the magnetometer. Similarly, the gyroscope sensor goes through a startup sequence via I^2C and can then acquire data continuously.

Requirements and Verification

Table 4: Requirements and Verification Table for Inertial Sensor Subsystem

Requirement	Verification
1. Both IMU devices shall communicate over I^2C to the MCU at a datarate of 400kHz.	**1A.** Using the MCU in debug mode, ensure that both IMU devices respond to I^2C write and read commands appropriately. **1B.** The MCU firmware will enter a fault state in the event of IMU communications failure, ensure that the MCU does not enter this fault state when operating conditions are acceptable (low rotation rates, low field strength, etc.).
2. The magnetometer shall be able to accurately detect the orientation of a magnetic field of between 0.25 and 0.65 Gauss.	**2A.** Using LASSI magnetic test cage, simulate the magnetic field conditions of low Earth orbit. Using an external MCU debugger, ensure that the magnetometer-reported values match external magnetometer sensors to within 5% of read value.
3. The gyroscope shall be able to accurately detect body rotation rates around any axis of <50 degrees per second.	**3A.** Using an external MCU debugger, ensure that the gyroscope-reported values match external gyroscope sensors to within 5% of read value.
4. The magnetometer shall be able to detect magnetic fields with a precision of less than or equal to 0.1μT per least significant bit of ADC readout.	**4A.** This is validated through part selection, testing COTS sensor performance to this degree is beyond the scope (and budget) of this course.

2.5 H-Bridges and Actuator Coils

The magnetorquer coils themselves are rather simple in their implementation. In order to perform magnetic rotations in orbit a spacecraft only needs to generate a magnetic field in the right orientation [1]. This breaks down into three simple solenoid coils, orthogonal to each other, rigidly mounted to the spacecraft body.

For our purposes, 32 AWG magnet wire will be wound around small 3d printed mandrels that will clip into spaces on the board. This will allow us to easily produce coils of reasonably precise dimensions. Due to the simple nature of the coil structure, we determined that it was best to wind each coil ourselves.

In order to be able to individually control each coil's direction, an H-bridge MOSFET structure is used to control each coil individually. This also allows the coils to be shorted closed, which is a useful emergency mode.

Requirements and Verification

Table 5: Requirements and Verification Table for H-Bridge and Actuator Subsystem

Requirement	Verification
1. X and Y axis coils shall be constructed to have a resistance within 3% of each other.	**1A.** Measure the resistance of each coil after their construction, ensure that the resistance values are within 3%.
2. All three coils must be mechanically compatible with LASSI specifications and the ADCS board mounting points.	**2A.** Ensure that the coils, when mounted, do not protrude off of the sides of the board. **2B.** Ensure that the Z axis coil does not protrude more than 3 centimeters above the top surface of the board.
3. Each coil shall be capable of having its current direction controlled by the MCU.	**3A.** Using an external magnetometer placed within 1 centimeter of the end of each coil (in turn), and an external MCU debugger commanding a coil test mode, ensure that the generated field direction is controllable by the MCU.
4. Each coil shall be capable of being shorted closed individually by the MCU.	**4A.** Using an external multimeter in continuity mode, probe the ends of each coil while it is being commanded short. Ensure that a very low resistance path is seen across the coil by the multimeter.

2.6 Processing

2.6.1 Hardware and Physical Design

Designing hardware for nanosatellites presents several unique environmental constraints that must be addressed in order for the module to be able to operate in a space environment. For the purposes of selecting an MCU, these constraints manifest themselves under the umbrella of power. Nanosatellites generally are low-power devices, operating at a maximum of only a few watts. This means that any module or subsystem inside that spacecraft must not consume too much power. Consuming large amounts of power in a small space results in localized heating. Due to the vacuum of space, this heat can only be released from the board through conduction through the board, and radiation to other parts of the spacecraft. Both of these processes are rather slow, and large thermal loads can damage the parts overtime.

Therefore, the MCU should operate in low-power constraints, support memory protection to prevent stray-writes and data corruption, support IO tamper detection since invalid data from defect sensors can render the ADCS system purposeless, and handle interrupts for handling requests from other sensors/hardware. Hence, we selected the STM32L5 series of 32 bit microcontrollers, given their extremely low-power performance, as well as our familiarity with their use in embedded systems for spaceflight.

Due to the ongoing semiconductors shortage, the only available package of the STM32L552 was a 0.5mm Ultra-Fine-Pitch Ball Grid Array (UFBGA-132) package. This package has 132 pins on its underside and measures 7x7mm in square dimension. Due to the extremely small feature size and tolerance requirements for a UFBGA package, immersion gold ENIG plating is required for the pads of this device in order to be sufficiently flat to solder BGA properly. Furthermore, in order to route tracks to the pads of the device, microvias-in-pad are required. This ***dramatically*** increases the cost of the board, and initial estimations from PCBWay had the whole thing at almost $400. Our solution to this is to break the STM32 out onto its own dedicated high-precision board, order that from a board house that costs less, and then use pin headers to mate the two devices together. This allows us to drop the main board to HASL plating and larger feature sizes, dropping the PCBWay cost to $75. A render of the MCU subcarrier board is shown in figure 3.

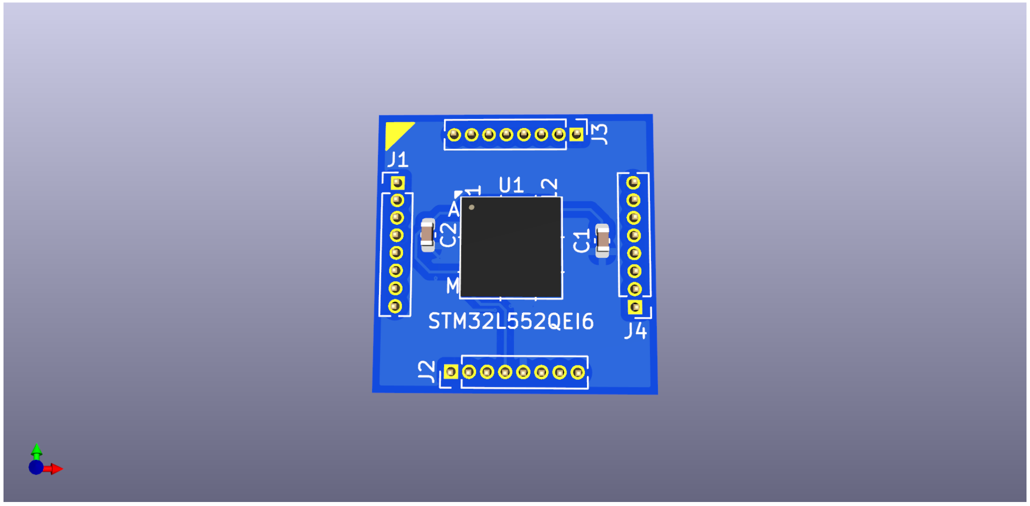

Figure 3: A render of the STM32L552 subcarrier module PCB. This board measures 2x2cm and is two layers thick.

The PCB must meet strict dimensional and geometry requirements under high-level requirement 1 (see table 1). This includes a pre-determined PCB shape and exact positioning of both the stack-through connectors on the top and bottom surface of the device and the mounting holes on the corners. Design was completed on the PCB prior to the board fabrication cost estimation, and a render of revision 1 is shown in figure 4.

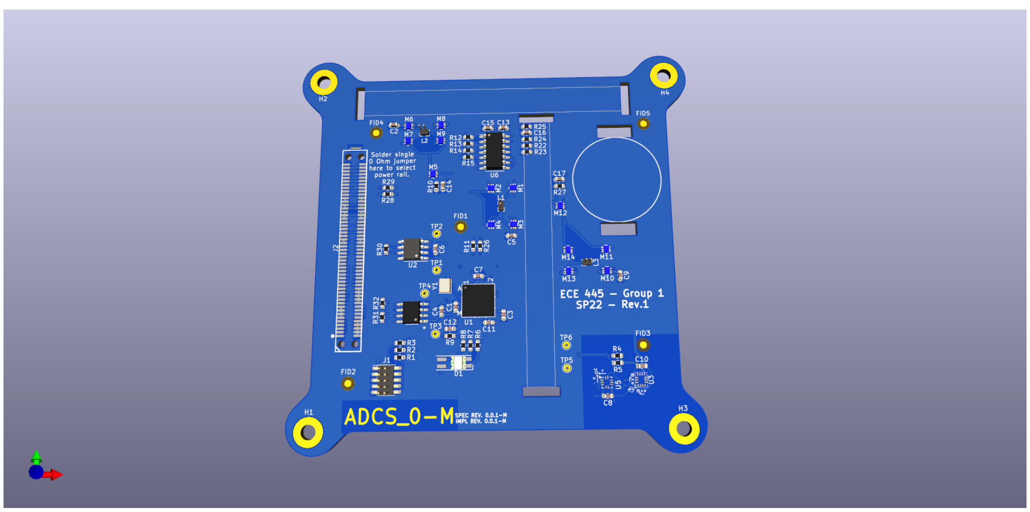

Figure 4: A render of revision 1 of the device. This version will not be produced. Not all components have models shown here.

The second revision of the board is rendered in figure 5. This version has the receiving holes for the pin header interface to the subcarrier module. This design is far cheaper to manufacture.

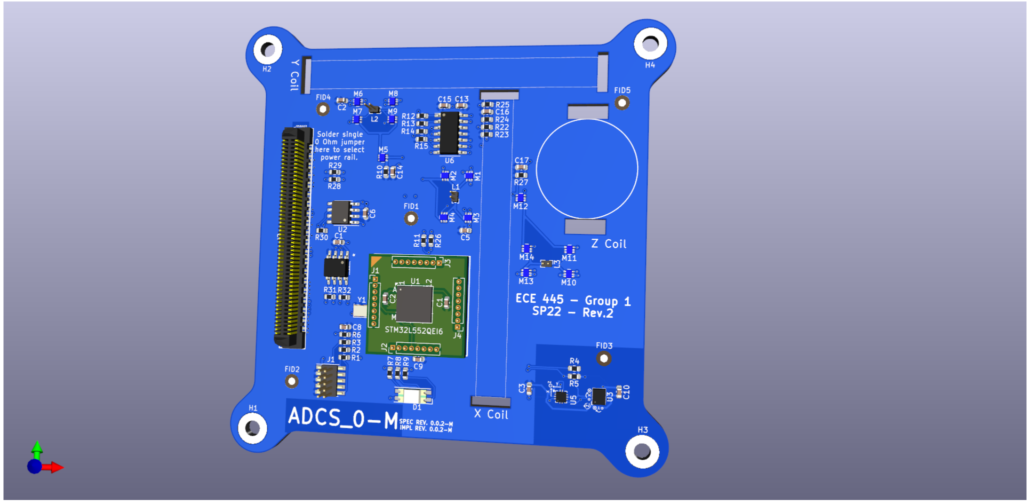

Figure 5: A render of revision 2 of the device. A render of the subcarrier module, shown as the green PCB, has been imported to show the two boards together.

This 4 layer board is circumscribed by a 90x90mm square, with 5mm of trench space on each side. The large J2 connector and its twin on the underside of the board, are Samtec ERM/F-8 100-pin connectors and serve as the stack-through interface between the satellite bus and our board. The two large empty rectangles book-ended by cuts into the board are the locations of the X and Y coils. The large circular space with cuts into the board on opposing sides is the Z axis coil location. The coils will mount with plastic clips into the cutout spaces in the board. The top layer of the device is flood-filled on the GND net, and provides some shielding between the signal and control traces and the magnetic coils. The bottom layer is flood-filled on the 3V3 net, providing easy access to power for devices and acting as an additional source of capacitance for power supply filtering. Note that the IMU devices, in the lower right-hand corner of figure 5, do not have flood fill. This is to prevent power plane noise being coupled into the sensors.

2.6.2 Firmware

The firmware running on the MCU does much of the heavy lifting of the module's capability. It must, at minimum, read data from the onboard sensors, communicate with external modules over the RS422/CAN, control and read currents from the constant-current drivers, perform self-test and calibration operations, and execute control algorithms using sensor data and current-driver actuators. Given the critical nature of the synchronization, interrupt handling, and communication tasks, we plan to use a Real Time Operating System (RTOS) to handle these tasks efficiently. The RTOS we plan to use is CMSIS-RTOS2, which has good compatibility with STM32 microcontrollers.

The firmware also has a state machine comprising of IDLE, FAULT, DETUMBLE, and TEST states, with optional SLEW, TARGET, DETERMINE states. These states are for performing necessary functions: help the satellite stay on course by adjusting its rotation (DETUMBLE), alert faulty behavior of on-board hardware (FAULT), self-diagnosis and provide complete report of the ADCS system (TEST).

Requirements and Verification

Table 6: Requirements and Verification Table for MCU Subsystem

Requirement	Verification
1. The MCU shall be capable of communicating over RS-422, CAN bus, and I^2C serial protocols.	**1A.** This is validated through other subsystem requirements.
2. The MCU shall be capable of executing self-test functions to ensure subsystems are operational and behaving within expected performance.	**2A.** Using an external debugger, ensure that the test functions execute and return values within determined accepted levels.
3. The MCU shall be capable of controlling the current set point of the constant current drivers.	**3A.** Using an external multimeter, measure the voltage between the MCU control signal output and ground, ensure that this voltage is within 1% of the commanded voltage by the firmware.
4. The MCU shall be capable of controlling the configuration of each coil H-bridge.	**4A.** Using an external MCU debugger, command each H-bridge into the forward, backward, short, and open configurations. Using a multimeter in the continuity mode, ensure that the H-bridge exhibits the commanded configuration.

2.7 Tolerance Analysis

The primary purpose of this device is to control the rotation rate of a spacecraft by applying torque to the spacecraft body. The device performs this task by generating magnetic fields which interact with the magnetic field around Earth. In order to provide useful control of the spacecraft, the torque generated must be controllable and must be strong enough to be useful to the mission.

For the purposes of this project, we are targeting performance of magnitude 1 order of magnitude to other comparable systems. For nanosatellites and cubesats of this class, a good analysis has been produced by Georgia Tech wherein they see ferrite-core magnetic field strength of between 12μT and 43.3μT [4]. Because their analysis was done with a ferrite core, a factor of derating has been included in our target of within 1 order of magnitude below.

The control torque that our system generates is formed by the interaction between our generated magnetic field and the magnetic field of Earth. The analysis for this is not unique or attributable to the work done in [4], however we are using their math almost verbatim for convenience.

$$\vec{T} = \vec{M}_{dipole} \times \vec{B} \tag{1}$$

In equation (1) the output torque $\vec{T}$ in N-m is shown to be equal to the cross product of the magnetic dipole generated by us, $\vec{M}$ in A-m^2, and the magnetic field around the Earth, $\vec{B}$. According to the National Oceanic and Atmospheric Administration, the geomagnetic field strength ranges from between roughly 25 and 65 μT [5]. We will use 25 μT as a conservative estimate for the magnetic field the system will encounter around the planet.

There are two primary areas where the tolerances of our system will be critical to project success, the sensitivity of our magnetic sensors, and the output torque of our actuators.

2.7.1 Magnetic Sensor Sensitivity

Generating arbitrary magnetic field vectors on orbit is a rather useless undertaking, it is far more useful to generate a magnetic field in the direction which will give the control torque requested by the MCU. In order to know where the control torque should be applied, the system must know where the Earth's field vector is relative to the spacecraft. This task is performed by the magnetometer sensor.

The geomagnetic field is very weak, and as such in order to accurately determine where the geomagnetic field is a sensitive sensor must be used. It is rather convenient for us then that this task is almost identical to the task of operating a compass inside a smartphone. Due to the demand generated by these devices, modern three-axis magnetometers with sensitivities sufficient for our application are readily available.

We have selected the Rohm Semiconductor BM1422AGVM three-axis magnetometer as our magnetic field sensing device. Table 7 is a comparison between the rated performance of the device and our required performance.

Table 7: Magnetometer Performance Requirements Comparison

Specification	**BM1422AGVM Rated Performance**	**Required Performance**
Measurable Magnetic Range:	$\pm 1200\mu$T	$\pm 65\mu$T
Magnetic Sensitivity:	0.042μT/LSB	0.1μT/LSB
Input Voltage Range:	1.7-3.6V	3.3V $\pm$0.1V
Operating Temperature Range:	-40 to +85°C	$\pm$40°C

Comparison between the rated performance of the device and our required performance.

As is shown by table 7, the BM1422AGVM meets or exceeds all relevant required parameters. In addition to this, the device contains a user-variable low-pass filter. Use of this filter will allow us to filter out high-frequency noise without consuming MCU processing time to do so.

2.7.2 Output Torque from Actuators

The output torque of the actuators, as shown in equation 1, is a function of the geomagnetic field and the field created by our system. It has been determined through experimentation that our group in this class cannot change the geomagnetic field. As such, we must focus our efforts on the fields created by our device. The magnetic dipole moment created by any one of our three magnetorquers is defined in equation 2.

$$\vec{M}_{dipole} = N \cdot I \cdot A \tag{2}$$

Where N is the number of loops of wire on the solenoid, I is the current through the wire in Amperes, and A is the cross-sectional area of the solenoid in m^2. For each of our three solenoid coils, we will wrap 1000 windings of wire around the coil. Coils X and Y will each have a mandrel diameter of 8mm and a length of 60mm, while coil Z will have a mandrel diameter of 6mm and a length of 20mm to accommodate a reduction in vertical height for that coil. The coils will not have a ferromagnetic core, but will instead have a core comprised of plastic. This allows us to assume the core is effectively free space.

In order to determine the current through each coil a simulation must be performed on the constant-current driver architecture. In order to perform the simulation, the Ohmic resistance of each coil must be calculated from the geometric parameters and the resistivity of copper, $1.68\times10^{-8}\ \Omega \cdot m$. We are using 32 AWG enameled copper wire, which is 3.2×10^{-8} m^2 in cross-sectional area.

$$R = \frac{\rho \cdot L}{A} \tag{3}$$

Equation 3 shows the relationship between the resistance of a wire, the length L of the wire in meters, the cross-sectional area of the wire in m^2, and the resistivity ρ of the wire in Ohm-meters.

$$L = N \cdot C \cdot 1.005 = N \cdot 1.005 \cdot (2\pi \cdot r) \tag{4}$$

Equation 4 shows the computation of the length of the wire as being the product of the number of wire wrappings N, the circumference of the coil $(2\pi \cdot r)$ in meters, and a 0.5% fudge factor to account for imperfect windings.

We can combine equations 3 and 4:

$$R = \frac{1.005\rho N(2\pi r)}{A} \tag{5}$$

$$R_{X\&Y} = \frac{1.005\rho N(2\pi r)}{A} = \frac{1.005(1.68 \times 10^{-8})1000(2\pi(0.004))}{3.2 \times 10^{-8}} = 13.261\Omega \tag{6}$$

The series resistance of coils X and Y, as calculated in equation 6, should be roughly 13.62 Ohms. The resistance of the Z axis coil requires an adjustment. Due to the shorter nature of the coil, the wire must be wrapped over itself in a series of layers in order to reach the desired number of turns. This increases the radius of each layer of wire and thereby increases its length. The width of the 32 AWG wire is 0.202 mm. Dividing the length by this gives the number of turns per layer, and adding the wire thickness to each successive layer radius will account for the increased length.

$$T_l = \frac{20}{0.202} = 99.059 \tag{7}$$

With almost exactly 100 turns per layer, the coil will be almost exactly 10 layers deep.

$$\sum_{n=0}^{9} T_l * C_n = \sum_{n=0}^{9} 99 * ((0.003 + (n * 0.00202)) * 2 * \pi) \approx 25.25m \tag{8}$$

Where T_l is the turns per layer and D_n is the circumference of layer n. Using calculation 8 of 25.25 meters of wire, the coil resistance can now be calculated.

$$R_Z = \frac{1.005\rho L}{A} = \frac{1.005(1.68 \times 10^{-8})25.25}{3.2 \times 10^{-8}} = 13.602\Omega \tag{9}$$

With equations 6 and 9 we have shown that despite having different geometries, the coil resistances will be essentially the same. This allows us to expect very similar performance out of the constant-current drives, as they can only drive as much current as the coil will draw.

Our device does not use an onboard regulator to generate a higher coil drive voltage, as such we drive the coils with 3.3 volts from the satellite power system. Our constant-current driver design is a simple dual op-amp design using an N-channel FET to drive current from the H-bridges.

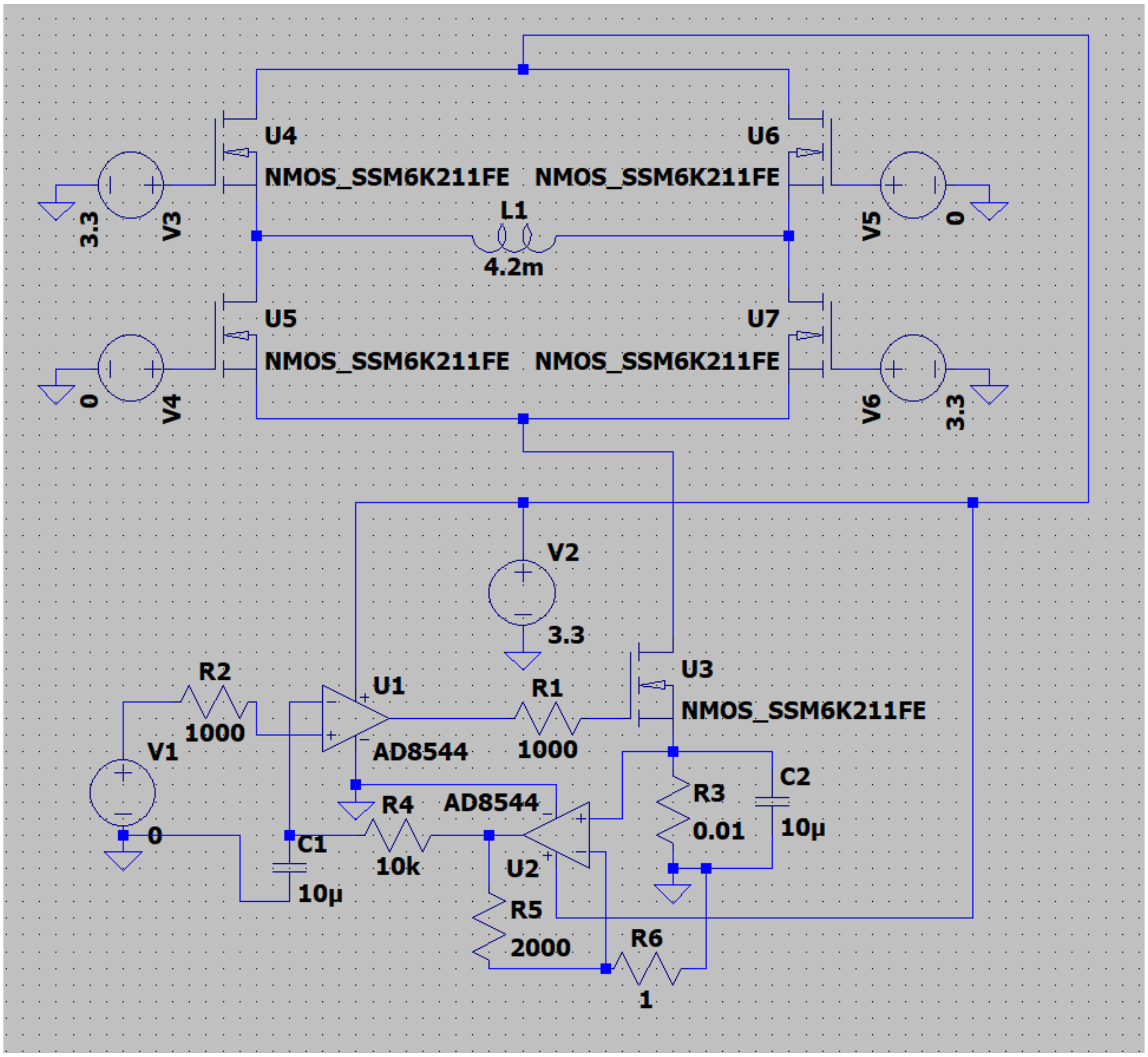

Figure 6: This is a schematic of the constant-current driver architecture. Source V2 is the 3v3 power supply rail, source V1 is the DAC output from the MCU and varies between 0 and 3v3, sources V3-V6 are GPIO outputs from the MCU and toggle only between 0 and 3v3.

Figure 6 shows a layout of the current driver architecture. The DAC output voltage from the MCU is represented as V1, this variable-level DC signal acts as the set-point for the driver system. This signal is fed into the non-inverting input of U1, an AD8544 op-amp. This op-amp outputs a signal onto the gate of U3, an N-channel FET which acts as the primary current driver.

U4-U7 are the H-bridge FETs, they are toggled between their conducting and non-conducting states by V3-V6, which represent the GPIO pins from the MCU which control them.

As current is driven through the system, the voltage from ground above the current sensing resistor R3 is tapped and sent to the non-inverting input of a second op-amp. This device acts only as a voltage level amplifier, taking the very small voltage drop across the current sensing resistor and amplifying it to a level which is useful.

In this situation the term useful means the voltage coming out of the amplifier represents as much of the full dynamic range of the current driver as possible. That is, when current is not flowing (the DAC output level is 0v) the sense amplifier outputs 0v, and when maximum current is flowing (the DAC output level is 3.3v) the sense amplifier outputs as close to 3.3v as possible.

It has been determined through simulation of this system in LTSPICE that the amplification ratio of the sense amplifier U2 should be approximately 2000 Ohms. This seems to result in the most linear response from the current driver, as seen in figure 7.

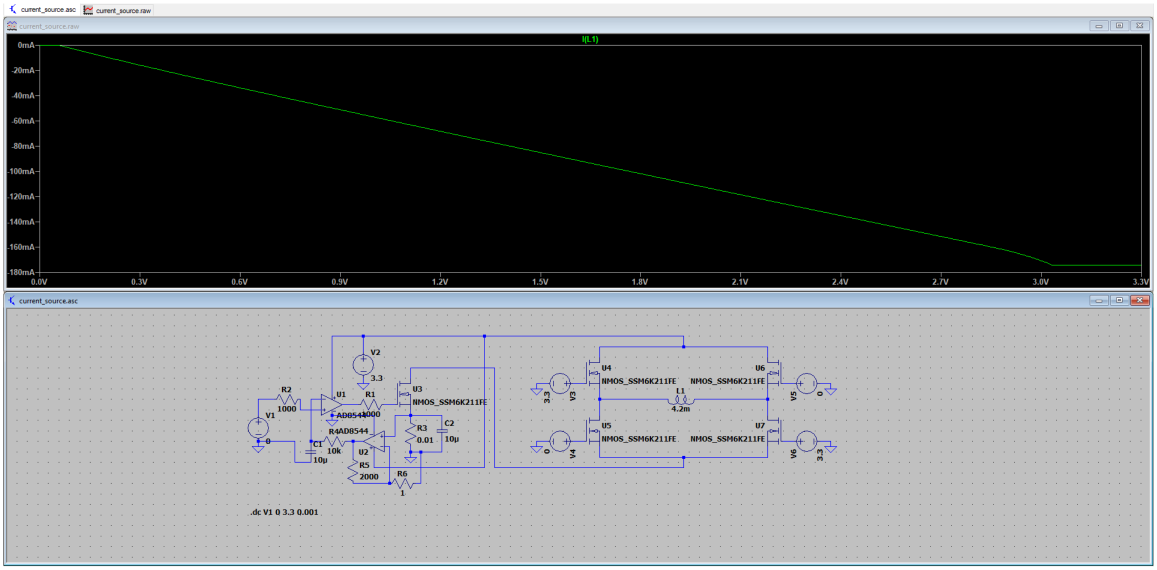

Figure 7: The output of an LTSPICE simulation of the H-bridge and constant current driver. In the simulation the source V1 is linearly swept from 0 to 3.3 volts. The green curve represents the current through the coil L1 during the input voltage sweep.

This simulation presents a validation of the constant current driver design as well as the H-bridge design. As each coil will have essentially the same resistance, the max current and dynamic range of each coil should be roughly the same. Care has been taken to simulate this system with the same op-amps and FETs as were sourced and purchased, as such it is expected that the system will see similar performance in hardware.

From here an analysis of magnetic field strength must be performed. We will use the maximum current produced by the constant current drive in the simulation as the drive current in this analysis, 175 mA. Equation 10 describes the related parameters of the B field created by the solenoid.

$$\vec{B} = \mu_0 \frac{N \cdot I}{l} \tag{10}$$

Where l is the length of the solenoid. For coils X and Y this is 60mm and for coil Z this is 20mm.

$$\vec{B}_{X\&YMAX} = \mu_0 \frac{1000(0.175)}{0.06} = 3.665mT \tag{11}$$

$$\vec{B}_{ZMAX} = \mu_0 \frac{1000(0.175)}{0.02} = 10.996mT \tag{12}$$

As shows in equations 11 and 12, the maximum magnetic field strength capable of being generated by the coils is significantly higher than the field created by the team at Georgia Tech. This is extremely good, as for the purposes of magnetic attitude control more field strength means more torque moment which means faster and more useful control.

3 Cost and Schedule

3.1 Labor

The hourly wage for a research project is estimated to be \$18 an hour, and our total time commitment is 15 hours/week for 12 weeks. We estimate a labor cost of \$8100 per person. Therefore, the total labor cost is estimated to be \$24,300. This is broken out in table 8.

Table 8: Labor Cost Analysis

Name	**Weekly Hours**	**Hourly Pay**	**Fudge Factor**	**Weeks**	**Cost (USD)**
Rick	15	18	2.5	12	8,100.00
Shrikar	15	18	2.5	12	8,100.00
Shamith	15	18	2.5	12	8,100.00
Total:					**\$24,300.00**

Per-person breakdown of labor costs for the project.

3.2 Parts

The cost of parts for this project is significant. Due to shortages in global semiconductor supply, the cost of many parts of the system have increased dramatically. Table 9 is a list of all parts already purchased. This list does not include the cost of shipping.

Table 9: Itemization of Parts Already Purchased

Part Name or Number	**Quantity**	**Cost (USD)**
AD8544WARZ Quad Op-Amp	10	22.19
ERM8-050 Stack Connector	1	11.01
ERF8-050 Stack Connector	1	10.38
SSM6k211FE NFET	30	13.80
RGB LED	10	2.40
32 AWG Copper Wire Spool	1	10.85
SN65HVD232 CAN XCVR	3	9.75
SN65HVD379 RS-422 XCVR	6	40.68
BMI270 IMU	4	59.96
BM1422AGMV IMU	10	66.10
STM32L552 MCU	2	25.08
ST Nucleo STM32L552 Devkits	*3*	*63.84*
19.2 MHz XO	*10*	*6.42*
Subtotal		*70.26*
Subtotal		272.20
Total		**\$342.46**

List and summation of cost of parts already purchased. Item listed in *italics* were purchased out of the ECE department-provided budget, all else was purchased by the group.

Table 10 is an estimation of the cost of parts not yet purchased.

Table 10: Estimated Itemization of Parts to be Purchased

Part Name or Number	**Quantity**	**Cost (USD)**
SMD Passives (Qty is sets of boards worth)	5	50.00
90x90mm 4-layer HASL main PCB	5	75.00
20x20mm 2-layer ENIG MCU carrier PCB with μVias-in-pad	5	66.00
Total		**$191.00**

3.3 Total Cost

Table 11: Total Cost

Category	**Cost (USD)**
Labor	24,300.00
Requisitioned Parts	*342.46*
Future Parts	*191.00*
Total	**$24,833.46**

This is a summation of the total costs we project to see for this project. Real costs, ones that involve actual purchasing, are marked in *italics*. Labor costs, which are a fabrication for this project as in fact we are paying to take this class, are in standard type.

3.4 Schedule

This schedule is notional and subject to change.

Table 12: Notional Schedule for Project

Week	Objectives	Notes
2/21	Design Document check, continue to layout PCB	Design Document check at 10AM on 2/21. Rick will continue to layout PCB. Shamith and Shrikar will continue to scope in firmware.
2/28	PCB Reviews	Rick will take point on PCB review. Shrikar and Shamith will have devkits by now to be able to begin prototyping firmware.
3/7	Order PCB and Teamwork Eval, Order Passives	PCB will be ordered this week at the latest, fabrication is anticipated to be at least 9 days and delivery another week or so. Firmware development will continue here. This is when passives will be ordered, as those quantities and values may change up to board ordering time.
3/14	*Spring Break*	*N/A*
3/21	Continue FW Development	Develop and unit test FW for operational states, RTOS should be operational and capable of executing arbitrary tasks. Boards in ideally late this week.
3/28	Assemble Boards, Flash, begin testing on real hardware.	Board assembly to be done by Pick-and-Place machine at LASSI, UFBGA package to be hand-soldered with BGA workstation. Firmware port and flashing to real hardware ideally by the end of the week.
4/4	I2C validation and sensor data validation, print mandrels and wind coils.	This week will be focused on making sure I2C works. Both IMU devices should send back data that matches external sensors. The coil mandrels and mounting hardware should be 3d printed by this week and the coils should be wound.
4/11	Current Driver and Firmware validation. Validation of self-test and calibration functions.	Validate that coils are drive-able by constant-current sources and that current is capable of being controlled and switched. Testing and tuning the self-test and calibration functions should happen here.
4/18	Continue to work through issues, mock demo to TA during meeting.	Basically a time-slip week, allows some time to fix issues as they crop up.
4/25	Continue to work issues and Demo.	Demonstration will be limited mostly to videos as our system relies on external hardware to operate.
5/2	Work on Final Paper.	Work on Final Paper.

A notional schedule of design and testing plans for the semester.

4 Ethics and Safety

4.1 Ethics

This project does not pose any significant ethical concerns on its own. It is by its nature incapable of doing anything on its own. However, because this is designed for use on a spacecraft, there are some additional ethical constraints that require address.

Prior to 2013, the United States federal government classified technology such as this project as "munitions" and restricted export of it and access to materials pertaining to it to U.S. citizens and green card holders only. Since then the related laws, the International Traffic in Arms Restrictions (ITAR), have been adjusted to remove this form of satellite technology from the list of munitions technology. [6]

Whenever an object is launched into orbit, two primary ethical questions are raised. How long will it take to come back down, and will it hit anything when it does? NASA guidelines require all cubesat-class satellites to re-enter the atmosphere within 10 years of launch, which is a very short lifetime for orbital debris. Because this requirement is enforced outside the scope of this project, we face no ethical constraints from it.

Similarly, orbital debris can sometimes survive interfacing with the atmosphere on re-entry. This occurs to parts of a spacecraft as a function of their orbital energy, material, and geometry. The U.S. FCC is the authority on restricting falling debris, they require the formulation of an Orbital Debris Assessment Report (ODAR) in order to grant a license to a satellite for the use of radio spectrum for communications. For our purposes, ethically we should only be working with materials that would be destroyed on re-entry. Effectively this means we should not be using stainless steel, titanium, or phenolic resin-impregnated silicate foams.

4.2 Safety Procedures

This project presents some risks to student safety. These risks primarily involve standard risks when working with PCBs and electrical equipment. Risks such as burn hazards, chemical exposure hazards from solder, flux, and PCB manufacturing residues, and other minor lab-related risks are assumed. Mitigation of said risks is the job of each involved engineer and student, lab safety is everyone's job.

There are several unique safety risks involved in this project. They are related to the testing and validation of the hardware we will develop. Use of LASSI space environment test equipment is proposed (as available from LASSI, we do not take priority over their other missions) for this project. Primarily this will involve the use of the Helmholtz Cage, a 3d magnetic field simulator. This test equipment uses compressed air, posing injection and aural hazards, as well as high-current drivers, posing burn hazards. These hazards will be mitigated through careful operation of the equipment by trained personnel, hearing protection PPE, and clear understandings of what parts of the system are "no touch" zones.

If time and resources permits, we will attempt to test the functionality of the device in a thermal vacuum chamber. This system is capable of pulling vacuum on hardware to validate its performance in a space environment. Use of the TVAC chamber presents compressed air injection hazards, cryogenic exposure hazards, electrical exposure hazards, and burn hazards. As such, it will only be operated by trained personnel, and the requisite DRS safety trainings will be required of all involved students.

Use of all specialized test equipment in the LASSI lab is contingent upon adherence to their hardware safety protocols and test procedures. These protocols have proven to be sufficient in protecting students, faculty, and staff operating this equipment.

References

[1] P. Wang, Y. Shtessel, and Y.-Q. Wang, "Satellite attitude control using only magnetorquers," in *Proceedings of Thirtieth Southeastern Symposium on System Theory*, 1998, pp. 500–504. DOI: 10.1109/SSST.1998.660124.

[2] I. Indir, K. Sever, I. Vnučec, and J. Lončar, "Design and optimization of air core magnetorquers for attitude control of leo nanosatellites," in *2021 International Symposium ELMAR*, 2021, pp. 135–138. DOI: 10.1109/ELMAR52657.2021.9550888.

[3] R. Stephens, "White paper: Expanding the usability of current-feedback amplifiers," Texas Instruments Incorporated, Dallas, Texas, Tech. Rep. SLYT099, Q3 2003, p. 7. [Online]. Available: https://www.ti.com/lit/an/slyt099/slyt099.pdf?ts=1644437138816.

[4] E. G. L. John Amin, "The design, assembly, and testing of magnetorquers for a 1u cubesat mission," Guggenheim School of Aerospace Engineering, Georgia Institute of Technology, Atlanta, GA, Dec. 2019, p. 14. [Online]. Available: https://www.ssdl.gatech.edu/sites/default/files/ssdl-files/papers/mastersProjects/AminJ-8900.pdf.

[5] A. S. M. P. A. C. B. M. N. B. H. A. W. V. R. S. M. A. T. N. G. M. T. Chulliat, "The us/uk world magnetic model for 2015-2020," National Geophysical Data Center, NOAA, Jan. 2015, p. 112. [Online]. Available: https://www.ngdc.noaa.gov/geomag/WMM/data/WMM2015/WMM2015_Report.pdf.

[6] P. Marks. "US no longer lists satellites as weapons." (), [Online]. Available: https://www.newscientist.com/article/dn23058-us-no-longer-lists-satellites-as-weapons/.